Multichannel quantum-defect theory of $n=2$ and 3 gerade states in H_2: Rovibronic energy levels

S. C. Ross
Department of Physics, University of New Brunswick, P.O. Box 4400, Fredericton, New Brunswick, Canada E3B 5A3

Ch. Jungen
Laboratoire Aimé Cotton du Centre National de Recherche Scientifique, Université de Paris–Sud, 91405 Orsay, France
(Received 6 July 1994)

Multichannel quantum-defect theory is applied to the gerade $n=2$ and 3 states of H_2. In the first paper in this series [Phys. Rev. A **49**, 4353 (1994)] we obtained the quantum-defect matrix of the strongly interacting $^1\Sigma_g^+$ double-minimum states of H_2 by fitting to the *ab initio* clamped-nuclei electronic energies of Wolniewicz and Dressler. This matrix was used in the second paper [Phys. Rev. A **49**, 4364 (1994)] to calculate the $N=0$ vibronic energies of the corresponding electronic states. In this paper we calculate the $N \geq 0$ rovibronic energies of the singlet and triplet gerade $n=2$ and 3 states of H_2. This *ab initio* treatment accounts for both singly and doubly excited channels and reproduces the rovibronic energies with almost the same accuracy as the more traditional coupled-equations approach. Additionally, the experimental singlet-triplet splittings for the f levels, and the evolution of these splittings with vibrational and rotational quantum numbers, are reproduced very well.

PACS number(s): 33.10.Cs, 33.10.Lb, 34.10.+x, 34.80.Kw

I. INTRODUCTION

In the preceding two papers [1,2] we developed the rovibronic multichannel quantum-defect theory (MQDT), accounting for l-mixing and coupling with states involving electronically excited cores. In the first of these (which we refer to as "RJ-I") we used the highly accurate potential-energy curves of Wolniewicz and Dressler [3] for the excited $^1\Sigma_g^+$ states of H_2 to extract a nondiagonal R-dependent quantum-defect matrix pertaining to the s and d Rydberg channels, associated with H_2^+ in its ground electronic state, and to the p Rydberg channel, associated with H_2^+ in its first excited state. In the second of the preceding papers (which we refer to as "RJ-II") we used this matrix to calculate the $J=0$ $^1\Sigma_g^+$ vibronic levels, including the levels of the EF and GK double-minimum states which experience strong nonadiabatic effects (as large as a couple of hundred wave-number units). In that work we achieved excellent agreement with experiment without having to laboriously evaluate the nonadiabatic functions required by the usual formalism. In the present paper we extend the treatment to levels with rotational quantum number N different from zero. Maintaining the restriction of our treatment to $l \leq 2$, this extension brings into play Π and Δ states. These are coupled with the Σ states by strong rotational-electronic (l uncoupling) interactions. The quality of the results we obtain here is comparable to that obtained in RJ-II, showing that the theory also accounts for these interactions, in addition to the pure vibronic interactions.

We also apply the theory with equal success to the triplet manifold of states. In the energy range we consider here, the triplet states are essentially unaffected by core-excited states, but do experience s-d mixing, as first recognized by Wakefield and Davidson [4] and most recently considered by Schins *et al.* [5]. The treatment of Schins *et al.* combines the high-quality *ab initio* potential-energy curves with a least-squares fitting to experimental data of the sharply peaked nonadiabatic coupling functions. Our calculation represents a fully *ab initio* treatment of these states, agreeing with experiment to within the order of 5–10 cm^{-1}, as in the singlet levels. We further show that slight adjustment (less than 0.002 at R_e) of the quantum-defect functions can improve this agreement to better than 0.2 cm^{-1}. We have also calculated the singlet-triplet splittings of the f-symmetry levels, achieving agreement with experiment of better than 1 cm^{-1}.

II. THEORY

In this work we apply the treatment outlined in RJ-II. The input data consist of the following.

(i) The *ab initio* potential-energy curves for the first two states of H_2^+, $1\sigma_g$, and $1\sigma_u$, as well as the corresponding adiabatic corrections for nuclear motion for these two states.

(ii) The R-dependent nondiagonal quantum-defect matrices for $\Lambda \leq l$.

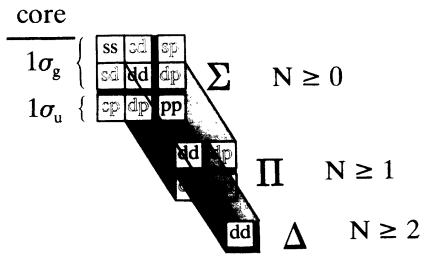

FIG. 1. Symbolized display of the electronic structure of the rovibronic K matrix [Eq. (4) of RJ-II]. See text for description.

In our calculations we restrict l to values less than or equal to 2 because higher l states are nonpenetrating and therefore do not strongly interact with the manifold considered here. For gerade states even-l values are associated with the $1\sigma_g$ ion core while odd-l values are associated with the $1\sigma_u$ core. Λ ranges up to the lesser of N and l. Figure 1 depicts this structure. In the body frame, Λ is a good quantum number with the results that the Σ, Π, and Δ blocks in Fig. 1 remain separate. However, as the electronic excitation is increased the Rydberg electron roams increasingly far from the core into the region wherein the lab frame is more appropriate for its description. In the lab frame Λ is no longer conserved, and the Λ blocks of Fig. 1 become mixed by the l-uncoupling interaction. In MQDT the transition between these two regimes is accounted for by the frame transformations of Eq. (14) of RJ-II.

Because the Pauli principle forbids the $(1\sigma_u)(2p\sigma_u)=(1\sigma_u)^2$ state in the triplet, the lowest $(1\sigma_u)(np\sigma_u)$ triplet state occurs for $n=3$, and lies to much higher energy than the range we are considering. For the triplet we therefore simplify the problem by neglecting all states built on the $1\sigma_u$ core; that is, by neglecting all elements involving p in Fig. 1. Further-

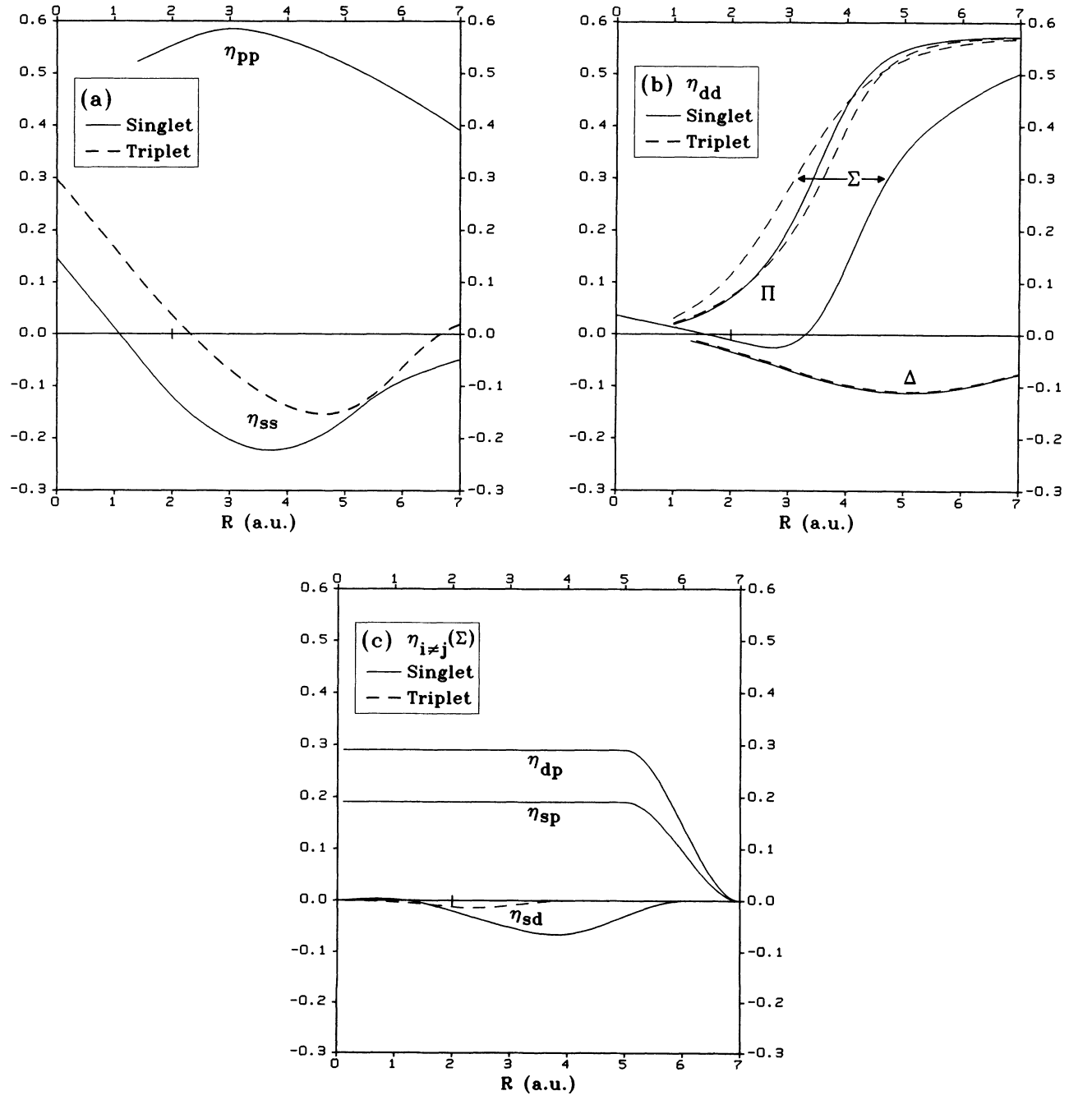

FIG. 2. Quantum-defect functions used in this work, those for Σ symmetry from RJ-I. Defects not shown are fixed to zero. (a) η_{ss} and η_{pp} defects for Σ symmetry. (b) η_{dd} defects for Σ, Π, and Δ symmetries. (c) Off-diagonal defects for Σ symmetry.

more, when f-symmetry levels are being considered, instead of e levels, the Σ block in Fig. 1 does not occur. In the e-symmetry states of the singlet, interactions involving doubly excited configurations are spread to all Λ values by the l-uncoupling interaction. This is seen formally in the summation on Λ in Eq. (4) of RJ-II, which is symbolized in Fig. 1 by the projection of the various Λ blocks onto each other, and leads to numerous possibilities of interactions between various levels occurring in the spectrum.

The evaluation of the elements of the rovibronic reaction matrix of Eq. (4) of RJ-II requires the knowledge of the R-dependent electronic reaction matrix which is defined in terms of the quantum-defect functions via Eq. (3) of RJ-II. Thus a variety of quantum-defect functions are needed. For the Σ states we have used the quantum-defect matrices determined in RJ-I and shown there in Figs. 3(a) and 3(b). The only exception is the triplet $\eta^{\Sigma}_{sd}(R)$ defect, for which we found two forms in RJ-I. In this work we use the second of these forms, which rises quadratically from $R=0$ to 2 a.u., before smoothly decreasing to zero at $R=0$ a.u., as described in Sec. IV A of RJ-I.

The quantum defects related to the Π and Δ states were derived from high-quality *ab initio* calculations by the same technique as used in RJ-I. For the singlet levels the Π states built on the $1\sigma_u$ core all lie well above the energy range considered here. Thus, although we could determine $\eta^{\Pi}_{pp}(R)$ from *ab initio* calculations such as those of Guberman [6], we instead simply fix it to zero. Likewise any interaction between the $(1\sigma_u)\varepsilon p\pi_u$ and $(1\sigma_g)\,\varepsilon d\pi_g$ channels will have no significant effect in this energy range and we therefore also fix $\eta^{\Pi}_{dp}(R)$ to zero. $\eta^{\Pi}_{dd}(R)$, the remaining Π defect, was directly determined from the *ab initio* Born-Oppenheimer potential-energy curve of Dressler and Wolniewicz [7] for the $I\,^1\Pi_g$ state. Similarly, the $\eta^{\Pi}_{dd}(R)$ defect for the triplet states was directly determined from the *ab initio* Born-Oppenheimer potential-energy curve for the $i\,^3\Pi_g$ state obtained by Kołos and Rychlewski [8]. Because of our restriction to $l\le 2$ the only Δ channel relevant to the present calculation is $(1\sigma_g)\,\varepsilon d\delta_g$. We obtained the singlet and triplet $\eta^{\Delta}_{dd}(R)$ defects from the *ab initio* Born-Oppenheimer potential-energy curves for the $J\,^1\Delta_g$ [9] and $j\,^3\Delta_g$ [10] states, respectively. Figure 2 shows all of the quantum defects used in the current work, while Fig. 3 shows the Born-Oppenheimer potential-energy curves for the states considered here.

Mulliken [11] has considered in detail the evolution with R of the $n=3$ orbitals of s and d character. From Table I of Mulliken's work it can be seen that at small and large R the molecular orbitals behave approximately as follows (small R forms given in the notation of RJ-I and RJ-II):

Small R		Large R
$3s\sigma_g$	→	$\sigma_g 3s$
$3d\sigma_g$	→	$\sigma_g 2p$
$3d\pi_g$	→	$\pi_g 2p$
$3d\delta_g$	→	$\delta_g 3d$

It is thus already clear that when the two H atoms approach each other from large distances, the $3d\sigma_g$ and $3d\pi_g$ components are obtained by promotion whereas the $3s\sigma_g$ and $3d\delta_g$ components are not. This behavior has its counterpart in the form of the diagonal quantum defects shown in Fig. 2 [$3s\sigma_g$ as η^{Σ}_{ss} in Fig. 2(a), and the $3d\lambda_g$ components as the η^{Λ}_{dd} in Fig. 2(b)]. Promotion is

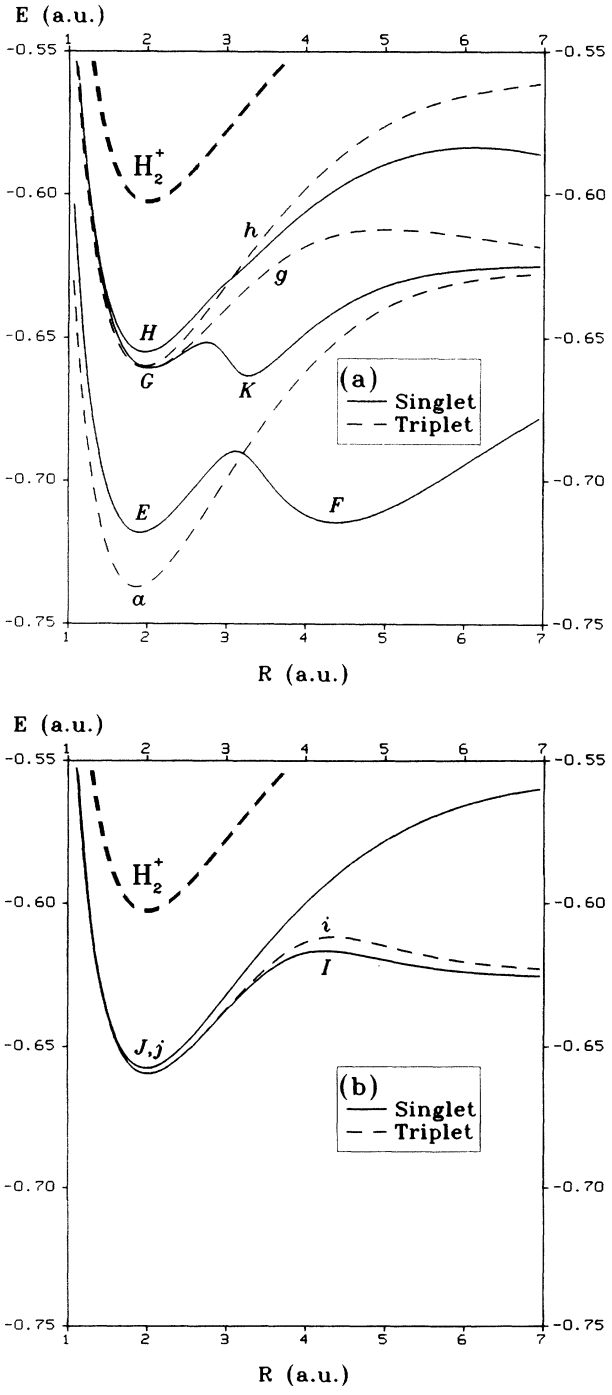

FIG. 3. Born-Oppenheimer potential-energy curves for singlet (solid curves) and triplet (dashed curves) states considered in this work, with their traditional labels. The $1\sigma_g$ state of H_2^+ is shown by the heavy dashed line. (a) Σ states. (b) Π (I and i states) and Δ (J and j states).

reflected in the μ quantum defect by a rise by one unit as R goes to infinity. The effect of promotion on the asymptotic behavior of the corresponding η defects is obtained by considering Eq. (4) of RJ-I:

$$\frac{\tan(\pi\nu)}{A(\nu)}+\tan(\pi\eta)=0\ , \tag{1}$$

where $A(\nu)$ is given by Eq. (5) of RJ-I. For promotion leading to $n=3$ at small R, the value of ν as $R\to\infty$ must be 2. Thus, because the first term in Eq. (1) for $\nu=2$ equals $4\pi/3$ as $R\to\infty$ for $l=2$, we must have $\eta_{dd}^{\Lambda}(R\to\infty)=-(1/\pi)\arctan(4\pi/3)=0.574\,59$. This is the asymptotic value to which the η_{dd}^{Σ} and η_{dd}^{Π} defects in Fig. 2(b) are seen to converge. Note that the η_{dd}^{Σ} singlet defect is somewhat special in that its rise occurs about 1.5 a.u. later than the triplet η_{dd}^{Σ} defect, while the singlet and triplet η_{dd}^{Π} defects remain close for all R values.

For small values of R the R dependence of the $l=2$ quantum-defect functions can be understood in a semiquantitative way by considering the medium- and long-range forces as acting on the d electron which only weakly penetrates the core. Retaining potential terms of the form r^{-n} up to $n=4$, the quantum defects can be expressed in first order (see, e.g., Ref. [12]) as

$$\mu_{dd}^{\Lambda}(\varepsilon,R)=\tfrac{1}{105}(1+2\varepsilon)\alpha(R)-\left[\frac{Q_2(R)}{105}+\tfrac{2}{735}(1+2\varepsilon)\tfrac{1}{3}[\alpha_{\parallel}(R)-\alpha_{\perp}(R)]\right](\Lambda^2-2)\ , \tag{2}$$

where $Q_2(R)$ is the molecular core quadrupole moment, and where $\alpha(R)=\frac{1}{3}[\alpha_{\parallel}(R)+2\alpha_{\perp}(R)]$ and $\frac{1}{3}[\alpha_{\parallel}(R)-\alpha_{\perp}(R)]$ are the spherical and nonspherical core dipole polarizabilities, respectively, and $\varepsilon=-1/\nu^2$. The polarizabilities are known accurately from theory for a wide range of R values (Ref. [13] and references therein). For the present purpose we must convert the μ quantum defects of Eq. (2) into η quantum defects. This is done by using $\nu=3$ in the identity

$$\tan(\pi\mu)=A_l(\nu)\tan(\pi\eta)\ , \tag{3}$$

where $A_l(\nu)$ is given by Eq. (5) of RJ-I. For $R=0$, Q_2 and $\frac{1}{3}[\alpha_{\parallel}(R)-\alpha_{\perp}(R)]$ are exactly zero while α has a small nonzero value. All three quantities increase rapidly as R becomes larger, and Eq. (2) leads to η_{dd}^{Λ} developing an increasing Λ structure [12], with the mean value of the Λ components also increasing.

Of course, the first-order expression in Eq. (2) is accurate only for very small R values and becomes inadequate as R increases. Furthermore, in this approximation the singlet and triplet quantum defects coincide exactly. Figure 4 compares the η defects obtained from Eqs. (2) and (3), with the corresponding *ab initio* ones used in this work. It can be seen that, with the single exception of the singlet η_{dd}^{Σ} defect (not shown in Fig. 4), Eq. (2) represents the η_{dd}^{Λ} quantum defects surprisingly well. They all meet quite smoothly with the *ab initio* defects around $R=1$ to 1.5 a.u. and remain in good agreement up to, and even somewhat beyond, the core internuclear distance, R_e^+, where the defects from Eq. (2) agree with the *ab initio* ones to within 0.008.

The singlet η_{dd}^{Σ} quantum defect is not shown in Fig. 4 since it follows a quite different route in this range of R values, as mentioned above. Even this deviation from the medium- and long-range force model can be understood, at least qualitatively, with reference to the medium-range polarization interaction. It is well known that polarization terms such as those in Eq. (2) effectively account for electronic core excitations provoked by the electric field of the Rydberg electron. However, in our approach, we *explicitly* account for excitation of the electronic $^1\Sigma_g^+$ channels built on the first excited $1\sigma_u$ core electronic state, through the singlet η_{dp}^{Σ} off-diagonal quantum-defect function. Therefore the bulk of the positive polarization contribution to the singlet η_{dd}^{Σ} quantum defect has already been removed, and this is why the corresponding curve in Fig. 2 lies considerably below its triplet analog, up to the point where the off-diagonal singlet η_{dp}^{Σ} defect goes to zero.

The rovibronic calculations were performed in essentially the same manner as the vibronic calculations as described in Sec. III D of RJ-II. The numbers of channels (indicated by the range of ν^+ values) that we used for

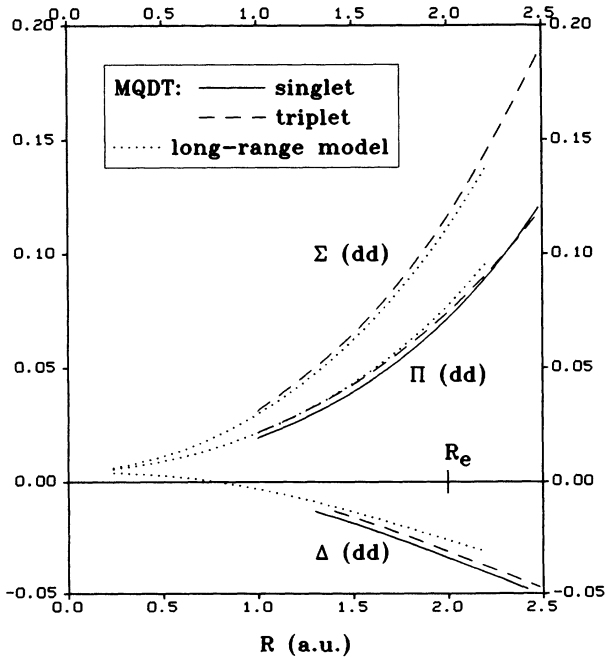

FIG. 4. Comparison of the η_{dd} quantum defect from Born-Oppenheimer potential-energy curves (singlet:solid curves, triplet:dashed curves) with that from the long-range model (dotted curves).

TABLE I. Breakdown of ionic vibrational basis (range of v^+ values) used in calculations.

		Singlet		Triplet	
core l[a]	N^+	e levels	f levels	e levels	f levels
$(1\sigma_g)s$	N	0:44		0:44	
$(1\sigma_g)d$	$N-2$	0:44	0:15	0:14	0:15
$(1\sigma_g)d$	N	0:44			
$(1\sigma_g)d$	$N+2$	0:44	0:15	0:14	0:15
$(1\sigma_u)p$	$N-1$	0:109			
$(1\sigma_u)p$	$N+1$	0:109			

[a]Electronic state of ion core and l value of Rydberg electron.

each value of N are given in Table I, broken down by the electronic state of the core, the l value of the Rydberg electron, and N^+.

Note that due to the restriction to $l \leq 2$, calculations for values of N greater than 2 do *not* involve a greater number of channels than those for $N=2$. Additionally, owing to the fact that higher l channels do not significantly penetrate the core, they do not significantly interact with other channels. Thus we do not anticipate serious difficulties from them when we perform calculations in energy ranges where they occur.

The involved nature of the programming has lead us each to develop an entirely independent computer program. The agreement of the results from these two programs lends confidence to the programming.

III. DISCUSSION OF RESULTS

A. General features

Tables II–V compare our *ab initio* calculated energies with experiment (see Tables for references and note that we have shifted Dieke's triplet energies [14] by -149.6 cm^{-1} [15]). The same data are displayed graphically in Fig. 5, where the observed and calculated levels are plotted. All of these levels were obtained by a single, unified, *ab initio* approach. Despite the fact that at least six different physical regimes can be distinguished in Fig. 5, the MQDT treatment accounts for the variety of physical effects with quantitative accuracy.

(i) At the lowest energies [Fig. 5(a)] the e-triplet manifold consists of the simple unperturbed $2s$ progression, while (ii) for the e-single manifold the $(1\sigma_u)(2p\sigma_u)$ doubly excited state adds a second potential minimum in this energy range. Tunneling through the barrier leads to the avoided crossings seen between the $(1\sigma_s)(2s\sigma_g)$ and $(1\sigma_u)(2p\sigma_u)$ levels lying below 105 000 cm^{-1}. The tunneling increases rapidly as the top of the barrier is

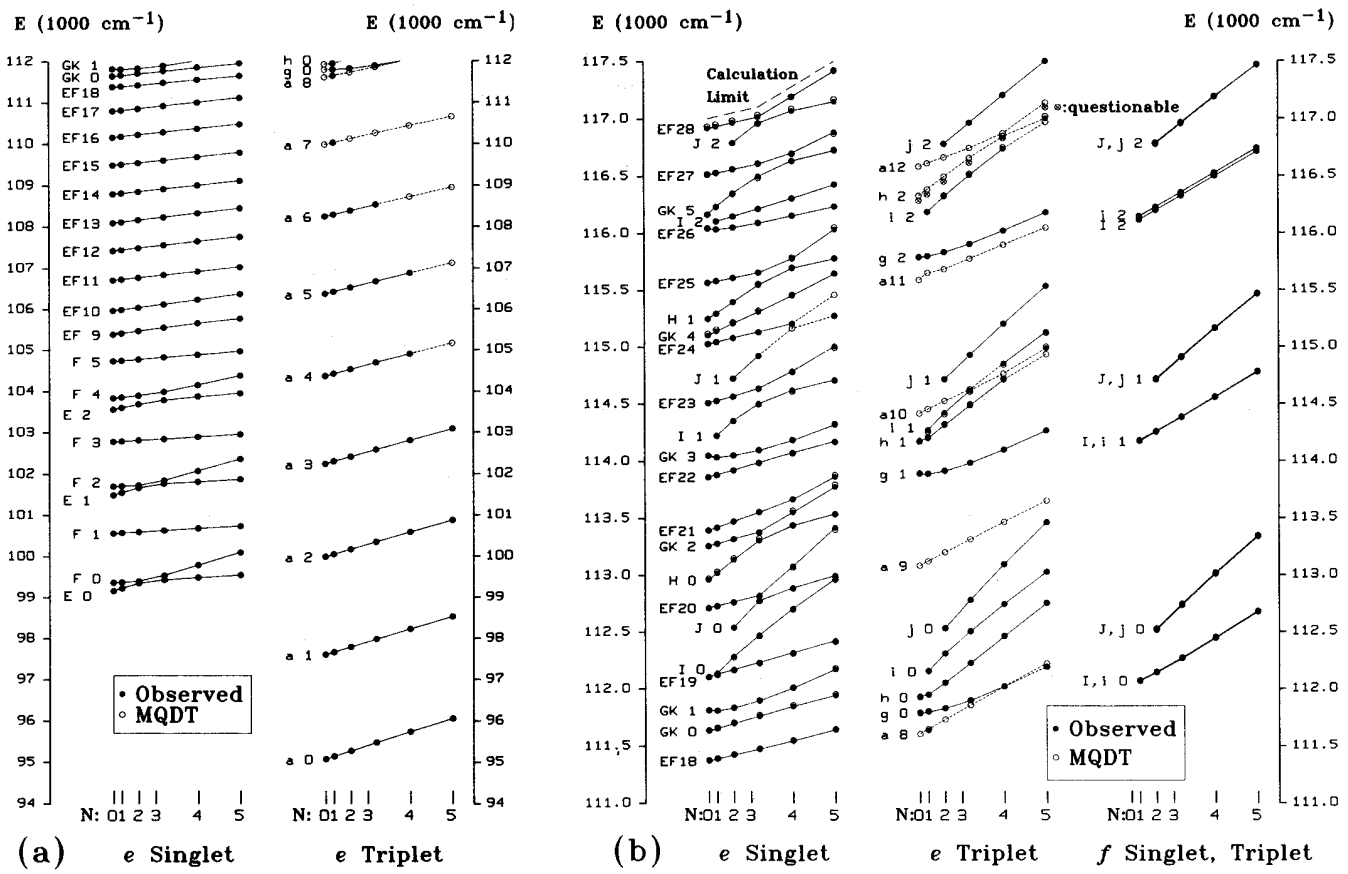

FIG. 5. Comparison of observed (solid circles, see Tables I–IV for references) and calculated (open circles, many obscured by observed points) term values. Lines are drawn to aid the eye. Observed levels for $h2$ ("×" in circle) are questionable. Energies relative to the $J=0$, $v=0$ level of the $X\,^1\Sigma_g$ ground state. (a) $E < 112\,000$ cm^{-1}. (b) $E > 111\,000$ cm^{-1}.

TABLE II. Comparison of observed and calculated rovibronic energies of singlet gerade e levels [parity $(-1)^N$] of H_2 (cm^{-1}).

Vibronic State[a]	N = 0		N = 1		N = 2		N = 3		N = 4		N = 5		Vibronic State
	Observed[b]	O-C[c]	Observed	O-C	Observed	O-C	Observed	O-C	Observed	O-C	Observed	O-C	
1 *E0*	99 164.7861[d]	4.4	99 228.2183[d]	4.6	99 354.572	4.5	99 437.16	1.3	99 485.98	1.3	99 546.83	1.2	*F0*
2 *F0*	99 363.92	1.3	99 376.04	1.3	99 400.52	1.3	99 542.778	4.6	99 791.34	4.6	100 098.27	4.6	*E0*
3 *F1*	100 558.92	0.1	100 570.81	0.1	100 594.82	0.2	100 630.71	0.1	100 678.52	0.1	100 738.19	0.2	*F1*
4 *E1*	101 494.749	5.0	101 554.041	5.0	101 671.649	4.8	101 768.53	0.3	101 816.10	0.3	101 875.04	0.5	*F2*
5 *F2*	101 698.93	0.3	101 710.80	0.3	101 735.03	0.5	101 849.412	4.9	102 081.05	4.7	102 367.17	4.4	*E1*
6 *F3*	102 778.28	-1.2	102 790.09	-1.1	102 813.85	-1.0	102 849.33	-1.0	102 896.49	-0.8	102 955.12	-0.7	*F3*
7 *E2*	103 559.59	-2.3	103 605.58	-2.5	103 690.13	-3.4	103 789.97	-4.4	103 876.35	-4.1	103 953.06	-3.3	*F4*
8 *F4*	103 838.54	0.0	103 857.83	0.4	103 903.00	1.3	103 995.21	2.1	104 159.79	1.4	104 386.90	0.1	*E2*
9 *F5*	104 730.61	-3.1	104 747.33	-2.9	104 780.20	-2.6	104 828.38	-2.1	104 891.67	-1.8	104 972.04	-0.8	*F5*
10 *EF9*	105 384.90	-0.1	105 415.23	-0.2	105 473.97	-0.4	105 556.84	-0.8	105 657.72	-1.1	105 770.18	-1.2	*EF9*
11 *EF10*	105 966.16	3.0	105 991.22	3.1	106 042.58	3.3	106 122.35	3.5	106 232.94	3.6	106 374.20	3.4	*EF10*
12 *EF11*	106 713.07	2.6	106 734.19	2.6	106 776.46	2.8	106 839.66	2.9	106 924.53	3.2	107 033.08	3.8	*EF11*
13 *EF12*	107 425.87	4.8	107 449.65	4.7	107 496.55	4.7	107 565.33	4.5	107 654.30	4.5	107 761.75	4.4	*EF12*
14 *EF13*	108 098.56	6.1	108 122.14	6.0	108 169.59	6.2	108 240.64	6.3	108 334.74	6.3	108 450.46	6.3	*EF13*
15 *EF14*	108 793.55	5.7	108 814.84	6.0	108 857.39	5.9	108 921.60	6.1	109 007.77	6.3	109 116.60	6.6	*EF14*
16 *EF15*	109 493.90	6.3	109 514.70	6.3	109 555.93	6.3	109 617.12	6.3	109 697.67	6.2	109 797.51	6.3	*EF15*
17 *EF16*	110 163.38	7.3	110 185.12	7.5	110 228.21	7.3	110 291.91	7.3	110 374.77	7.1	110 475.26	7.0	*EF16*
18 *EF17*	110 794.19	6.2	110 815.23	6.4	110 857.53	6.6	110 921.66	6.9	111 007.66	7.4	111 114.66	7.7	*EF17*
19 *EF18*	111 370.69	-4.6	111 387.13	-4.5	111 420.72	-4.5	111 472.60	-4.4	111 544.97	-4.2	111 641.89	-3.4	*EF18*
20 *GK0*	111 628.81	-7.5	111 650.27	-7.3	111 693.73	-7.9	111 759.92	-9.2	111 845.27	-10.4	111 941.78	-11.4	*GK0*
21 *GK1*	111 812.665	1.1	111 805.139	-2.5	111 827.768	-5.3	111 893.099	-6.8	112 005.510	-7.9	112 170.006	-9.2	*GK1*
22 *EF19*	112 106.09	7.2	112 126.13	7.1	112 167.83	7.3	112 230.94	7.2	112 315.97	6.9	112 421.49	6.4	*EF19*
23 *I0*			112 135.260	3.7	112 282.303	7.1	112 471.058	8.9	112 703.728	9.9	112 966.347	8.2	*EF20*
24 *J0*					112 536.772	1.1	112 774.608	5.0	112 887.08	5.3	112 996.40	8.8	*I0*
25 *EF20*	112 711.80	5.3	112 729.14	5.4	112 763.87	5.3	112 818.87	5.9	113 078.218	11.1	113 415.49	14.7	*J0*
26 *H0*	112 957.57	-10.3	113 016.73	-11.7	113 134.08	-14.6	113 303.44	-20.8	113 434.33	-3.0	113 536.24	2.2	*EF21*
27 *GK2*	113 258.24	2.7	113 277.69	1.5	113 316.60	1.4	113 378.41	2.8	113 548.77	-3.0	113 772.52	-18.4	*GK2*
28 *EF21*	113 393.50	2.5	113 418.81	1.7	113 470.58	0.3	113 550.35	-1.6	113 662.45	-2.2	113 860.46	-16.4	*H0*
29 *EF22*	113 861.40	4.7	113 879.34	4.0	113 920.31	3.5	113 987.54	4.0	114 075.22	5.4	114 173.43	6.2	*EF22*
30 *GK3*	114 044.66	-1.3	114 030.86	-2.5	114 046.36	-3.2	114 093.58	-4.6	114 180.25	-6.7	114 318.58	-8.0	*GK3*
31 *I1*			114 223.95	2.5	114 353.75	3.4	114 502.49	7.8	114 620.01	11.4	114 711.68	5.9	*EF23*
32 *EF23*	114 510.55	4.6	114 528.53	4.3	114 566.16	4.1	114 636.18	4.5	114 785.41	7.4	115 004.91	13.5	*I1*
33 *J1*					114 721.42	0.6	114 923.50	2.4	*115 164.96*[e]		115 275.77	0.7	*EF24*
34 *EF24*	115 024.83	1.3	115 044.03	1.7	115 079.95	1.3	115 131.12	1.0	115 207.34	3.4	*115 459.50*[e]		*J1*
35 *GK4*	115 099.84	-16.1	115 136.70	-15.2	115 207.34	-12.0	115 310.01	-10.7	115 450.26	-8.3	115 646.21	-0.6	*GK4*
36 *H1*	115 251.52	5.0	115 296.88	2.6	115 393.84	-1.8	115 544.94	-8.8	115 692.88	-6.3	115 777.68	-5.0	*EF25*
37 *EF25*	115 563.70	-1.4	115 577.68	-1.3	115 606.77	-1.2	115 653.92	-1.0	115 777.13	-10.0	116 034.92	18.4	*H1*
38 *EF26*	116 041.59	-1.4	116 031.65	-2.1	116 047.33	-2.5	116 088.60	-3.0	116 151.54	-3.4	116 232.41	-4.0	*EF26*
39 *I2*			116 103.65	0.2	116 148.36	0.5	116 214.23	0.2	116 305.38	-0.8	116 424.46	-3.4	*GK5*
40 *GK5*	116 164.81	1.7	116 233.76	3.1	116 349.14	6.0	116 495.05	11.3	116 633.51	2.1	116 721.99	-4.8	*EF27*
41 *EF27*	116 508.24	-5.2	116 523.55	5.2	116 554.55	-4.9	116 604.10	-3.9	116 701.85	5.7	116 883.64	14.2	*I2*
42 *J2*					116 787.75	1.9	116 960.16	1.2	117 068.80	-18.6	117 148.71	-20.9	*EF28*
43 *EF28*	116 915.41	-16.8	116 931.86	-17.3	116 964.40	-19.0	117 016.19	-17.2	117 193.20	1.5	117 413.90	-9.3	*J2*

[a] Levels numbered in energy order. Due to significant mixing of some levels the vibronic labels are sometimes of only notational convenience. The approximate locations of avoided crossings are indicated by the X symbols.
[b] Observed term values in cm^{-1}, relative to the $N = 0$, $v = 0$ level of the $X\ ^1\Sigma_g^+$ ground state, from Ref. [16].
[c] Observed minus calculated values in cm^{-1}.
[d] Ref. [20]. $N = 1$ value obtained by adding $N = 1$, $v = 0$ $X\ ^1\Sigma_g^+$ ground state energy of 118.4868 cm^{-1} [21] to Q(1) transition of Ref. [20].
[e] Calculated value only, given in italics with no observed minus calculated value.

TABLE III. Comparison of observed and calculated rovibronic energies of singlet gerade f levels [parity $-(-1)^N$] of H_2 (cm^{-1}).

Vibronic State[a]	N = 1		N = 2		N = 3		N = 4		N = 5	
	Observed[b]	O-C[c]	Observed	O-C	Observed	O-C	Observed	O-C	Observed	O-C
1 *I0*	112 072.886	-0.9	112 147.640	-1.1	112 272.108	-1.2	112 449.120	-1.4	112 679.102	-1.6
2 *J0*			112 525.979	-0.6	112 743.568	-0.3	113 018.385	-0.1	113 346.57	0.2
3 *I1*	114 172.13	-0.6	114 252.86	-0.8	114 379.11	-1.0	114 552.96	-1.1	114 775.09	-1.3
4 *J1*			114 718.24	-0.0	114 914.55	0.3	115 166.62	0.6	115 470.26	0.9
5 *I2*	116 114.42	0.1	116 197.52	-0.1	116 324.01	-0.2	116 494.72	-0.3	116 709.73	-0.5
6 *J2*			116 787.20	0.7	116 963.16	0.9	117 191.62	1.2	*117 467.44*[d]	

[a] Levels numbered in energy order.
[b] Observed values in cm^{-1}, relative to the $J = 0$, $v = 0$ level of the $X\ ^1\Sigma_g^+$ ground state, from Ref. [16].
[c] Observed minus calculated values in cm^{-1}.
[d] Calculated value only, given in italics with no observed minus calculated value.

TABLE IV. Comparison of observed and calculated rovibronic energies of triplet gerade e levels [parity $(-1)^N$] of H_2 (cm^{-1}).

Vibronic State[a]		N = 0 Observed[b]	O-C[c]	N = 1 Observed	O-C	N = 2 Observed	O-C	N = 3 Observed	O-C	N = 4 Observed	O-C	N = 5 Observed	O-C	Data Source
2a	*a0*	95 076.298	-0.8	95 142.982	-0.8	95 275.792	-0.8	95 473.729	-0.7	95 735.224	-0.7	96 058.350	-0.7	Jungen *et al.*[d]
		076.40	-0.7	143.07	-0.7	275.90	-0.7	473.84	-0.6	735.33	-0.6	058.44	-0.6	Dieke[e]
	a1	97 600.619	-1.3	97 664.044	-1.3	97 790.352	-1.3	97 978.589	-1.3	98 227.243	-1.3	98 534.463	-1.3	Jungen *et al.*
		600.72	-1.2	664.14	-1.2	790.46	-1.2	978.70	-1.2	227.35	-1.2	534.54	-1.2	Dieke
	a2	99 989.00	-1.5	100 049.26	-1.5	100 169.29	-1.5	100 348.13	-1.4	100 584.32	-1.4	100 876.14	-1.3	Dieke
	a3	102 245.13	-1.5	102 302.30	-1.5	102 416.21	-1.5	102 585.89	-1.5	102 809.92	-1.5	103 086.73	-1.5	Dieke
	a4	104 372.03	-0.9	104 426.18	-0.9	104 534.05	-0.9	104 694.73	-0.9	104 906.60	-1.2	*105 169.72*[f]		Dieke
	a5	106 371.62	-0.5	106 422.75	-0.5	106 524.67	-0.5	106 676.09	-1.0	106 876.61	-0.7	*107 124.68*		Dieke
	a6	108 244.45	-0.5	108 292.56	-0.6	108 388.55	-0.6	108 531.13	-0.9	*108 720.60*		*108 953.27*		Dieke
	a7	*109 989.98*		110 034.76	-0.4	*110 125.06*		*110 258.91*		*110 435.63*		*110 653.21*		Dieke
	a8	*111 604.30*		111 634.99	-11.4	*111 730.08*		*111 854.64*		*112 018.99*		*112 221.25*		Dieke
	a9	*113 082.62*		*113 121.42*		*113 198.59*		*113 313.38*		*113 464.60*		*113 650.66*		present calculations
	a10	*114 415.78*		*114 451.05*		*114 521.18*		*114 625.37*		*114 762.42*		*114 930.72*		present calculations
	a11	*115 589.43*		*115 651.00*		*115 682.95*		*115 775.20*		*115 896.26*		*116 044.41*		present calculations
	a12	*116 581.68*		*116 608.39*		*116 661.32*		*116 739.56*		*116 841.73*		*116 965.94*		present calculations
3a	*h0*			111 948.156	2.1			112 223.276	-2.0					Jungen *et al.*
		(111 871.88	-54.5)[g]	(933.11	-13.0)	112 050.12	-0.6	223.34	-2.0	112 457.82	-3.1	*112 753.79*		Dieke
	h1	(114 140.61	-30.4)	114 198.05	-7.2	114 312.11	-9.4	114 482.28	-10.6	114 707.06	-11.6	114 984.50	-12.8	Dieke
	h2					(116 448.25	-43.4)	(116 611.43	-43.3)	(116 827.05	-42.5)			Dieke
		116 326.95		*116 382.04*		*116 491.68*		*116 654.71*		*116 869.50*		*116 133.93*		present calculations
3d	*g0*			111 796.467	-4.8	111 826.498	-2.5	111 896.638	-1.5	112 017.210	-1.0			Jungen *et al.*
		(111 798.58	8.2)	796.59	-4.7	826.63	-2.4	896.72	-1.5	017.36	-0.9	112 190.84	-0.8	Dieke
	g1	113 886.39	-5.4	113 883.81	-5.5	113 910.96	-3.5	113 980.42	-2.1	114 097.34	-1.5	114 263.83	-1.0	Dieke
	g2	115 784.97	-6.4	115 794.54	-4.8	115 829.40	-3.4	115 901.99	-2.3	116 017.52	-1.6	116 178.49	-1.0	Dieke
3e	*i0*			112 153.630	0.8	112 310.889	0.8	112 503.692	0.5					Jungen *et al.*
				153.70	0.9	311.00	0.9	503.73	0.5	112 741.04	0.5	113 027.04	0.5	Dieke
	i1			114 269.16	11.7	114 419.39	11.2	114 614.15	10.5	114 850.24	10.1	115 129.19	10.5	Dieke
	i2			116 182.22	-3.3	116 319.29	-7.5	116 504.19	-11.6	116 731.46	-15.2	116 999.71	-17.2	Dieke
3f	*j0*					112 529.550	-1.2	112 779.414	-0.5					Jungen *et al.*
						529.65	-1.1	779.49	-0.4	113 092.96	0.0	113 460.59	0.4	Dieke
	j1					114 712.08	-0.7	114 924.70	0.0	115 201.04	0.6	115 533.40	1.3	Dieke
	j2					116 777.92	-0.3	116 962.18	0.2	117 203.90	0.8	117 498.63	1.3	Dieke

[a] Dieke's label for the electronic states, followed by the traditional labelling of the vibronic states.
[b] Observed values in cm^{-1}, relative to the $J = 0$, $v = 0$ level of the $X\ ^1\Sigma_g^+$ ground state.
[c] Observed minus calculated values in cm^{-1}.
[d] Ref. [18].
[e] Values from Ref. [14] minus 149.6 cm^{-1} [15].
[f] Calculated values from current work, given in italics with no observed minus calculated value.
[g] Observed levels in parenthesis are questionable.

TABLE V. Comparison of observed and calculated rovibronic energies of triplet gerade f levels [parity $-(-1)^N$] of H_2 (cm^{-1}).

Vibronic State[a]		N = 1 Observed[b]	O-C[c]	N = 2 Observed	O-C	N = 3 Observed	O-C	N = 4 Observed	O-C	N = 5 Observed	O-C	Data Source
3e	*i0*	112 066.652	-1.0	112 140.816	-1.2	112 264.876	-1.5	112 441.765	-1.7			Jungen *et al.*[d]
		066.82	-0.8	140.97	-1.1	264.97	-1.4	441.73	-1.8	112 671.83	-1.9	Dieke[e]
	i1	114 180.18	0.1	114 259.01	-1.1	114 384.33	-1.3	114 557.72	-1.5	114 779.60	-1.8	Dieke
	i2	116 145.69	-0.6	116 227.91	-0.8	116 353.37	-1.0	116 523.33	-1.1	116 738.08	-1.4	Dieke
3f	*j0*			112 513.945	-1.4	112 732.183	-1.2					Jungen *et al.*
				514.02	-1.4	732.32	-1.0	113 007.64	-0.8	113 336.26	-0.6	Dieke
	j1			114 706.74	-0.9	114 904.56	-0.6	115 158.21	-0.2	115 463.41	0.0	Dieke
	j2			116 776.30	-0.1	116 954.80	-0.1	117 186.35	0.2	117 467.10	0.5	Dieke

[a] Dieke's [14] label for the electronic states, followed by the traditional labelling of the vibronic states.
[b] Observed values in cm^{-1}, relative to the $J = 0$, $v = 0$ level of the $X\ ^1\Sigma_g^+$ ground state.
[c] Observed minus calculated values in cm^{-1}.
[d] Ref. [18].
[e] Values from Ref. [14] minus 149.6 cm^{-1} [15].
[f] From "calculated" values of Tables VIII and IX of Ref. [19].

reached, resulting in ever stronger interaction and wider avoided crossings (cf. $E0$-$F0$, $E1$-$F2$, and $E2$-$F4$). (iii) Above this, the e-singlet enters another regime as the two series blend into a single progression of mixed singly and doubly excited character.

Just above 111 000 cm^{-1} [Fig. 5(b)] both the e-singlet and e-triplet manifolds experience the onset of the $n=3$ states. (iv) In the singlet the spectrum exhibits a complicated pattern of avoided crossings of sufficient strength to separate the interacting levels and to produce a deceptively clean appearance. The spreading of the various clumps of levels is due to the effects of l uncoupling, but this is rather obscured by the other interactions. (v) In the triplet manifold the only mixing is *sd* mixing, which is sufficiently weak to allow may levels to approach each other closely and thus result in a somewhat more congested appearance. The weakness of this mixing, however, does allow the l uncoupling to be clearly seen, in groups such as the levels from $g1$ to $j1$ lying near 114 000 cm^{-1} which spread increasingly apart as rotation increases. (vi) Finally, the singlet and triplet f levels exhibit almost identical patterns which reflect the effects of pure l-uncoupling interaction.

Altogether the experimental e-symmetry levels are reproduced extremely well, as indicated in the summary Table VI. Here the rms errors of the MQDT calculated energies are shown, along with the range of errors seen in Tables II–V. Equivalent results for the coupled-equations calculations of Yu and Dressler [16] are given for comparison. Because the coupled-equations energies always lie above the true values, whereas the MQDT results scatter on either side, the simple rms error is not appropriate for comparing the results obtained from the two treatments. To this end the rms *about the average deviation* is also shown in the table. This, together with the ranges of the errors, indicate that our current MQDT results for the e-symmetry levels are only a factor of 2–2.5 times worse than those obtained using the coupled-equations approach. Because our fitting of the quantum defects involved here only reproduces the Born-Oppenheimer potential-energy curves to within 8 cm^{-1} (1.7-cm^{-1} rms) in any case, the rms error of the e-singlet and e-triplet vibronic energy levels of 6.6 cm^{-1} and 5.0 cm^{-1}, respectively, is entirely satisfying.

The f-singlet and f-triplet levels shown at the right of Fig. 5(b) are examples of pure l uncoupling which MQDT is ideally suited to treat. The lack of electronic configuration mixing for these levels allows the full accuracy of the theory to reveal itself, devoid of inaccuracies resulting from any inadequacies in the fitting of the interaction quantum defects in RJ-I. Thus for these levels the quality of agreement between the calculated and observed levels is of the order of 1 cm^{-1}, with all differences being less than 2 cm^{-1}. For the f-singlet levels the coupled-equations technique [16] is about four times worse, with the largest difference being 9.8 cm^{-1}. Essentially, the coupled-equations results are no better or worse for the f-symmetry levels than they were for the e-symmetry ones.

B. Singlet-triplet splittings

Figure 6 compares our calculated singlet-triplet splittings for the f-symmetry levels with the experimental splittings (obtained from the data given in Tables III and V). The MQDT results are in excellent agreement with experiment, all lying within better than 1.0 cm^{-1} (rms deviation 0.7 cm^{-1}) of the observed differences. Note that this accuracy is almost as good as the experimental results obtained by Miller and Freund in their pioneering singlet-triplet anticrossing experiments on these same states [17]. It is only recently that this accuracy has been surpassed by experiment [18].

The absence of the $n=2$ doubly excited state in the triplet manifold means that there is not a one-to-one correspondence between singlet and triplet levels of e symmetry. Thus for e symmetry the singlet-triplet splittings have no evident meaning and we do not consider them.

C. Fine adjustment of triplet quantum defects

It is possible to perform a fine adjustment of the *ab initio* quantum defects to further improve the agreement with experiment. Although such an adjustment is not a

TABLE VI. Rms errors of calculated energies from MQDT (present work) and coupled-equation (Ref. [16]) approaches.

		Singlet				Triplet			
		rms[a]	range[b]	num.[c]	rms-avr[d]	rms	range	num.	rms-avr
e levels	MQDT[e]	6.6	−20.9:18.4	(247)	6.6	5.0	−17.2:11.2	(82)	4.6
	CE[f]	4.2	0.1:11.8	(247)	2.8				
f levels	MQDT	0.8	−1.6:1.2	(26)	0.7	1.1	−1.9:0.5	(27)	0.6
	CE	5.5	0.9:9.8	(26)	3.2				

[a]Root-mean-square error of theoretical calculations.
[b]Range of deviations with experiment (cm^{-1}).
[c]Number of levels used in calculating the rms error.
[d]The rms deviation (cm^{-1}) around the average deviation.
[e]Present work.
[f]Coupled equations [16] statistics calculated for the same levels as used for the MQDT levels.

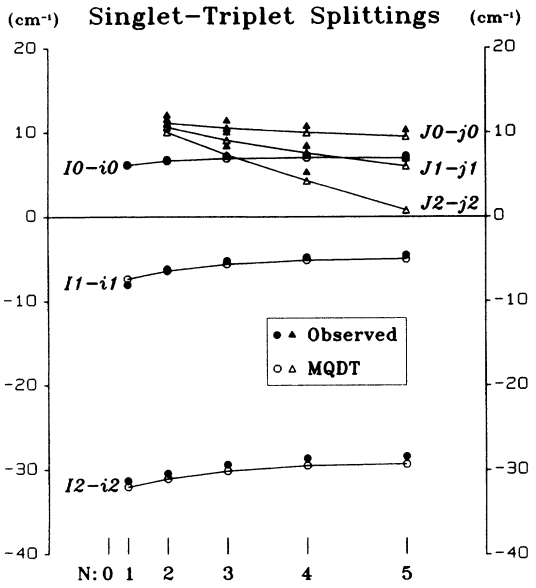

FIG. 6. Comparison of experimental and MQDT singlet-triplet splittings for the f-symmetry levels.

principle aim of this work, we do wish to illustrate this possibility and to this end have performed a limited least-squares fitting involving only the 17 $v=0$ triplet levels reported by Jungen *et al.* [18]. These levels have an absolute accuracy of 0.05 cm^{-1} and we used them in a least-squares fitting of the triplet quantum defects around R_e. This was done by representing the quantum defects in the region near R_e as quadratic functions of R. The quadratic coefficients were fixed to values determined from the *ab initio* values, while the values for $R=2$ a.u. and the linear coefficients were adjusted in the fitting. The fitted defects are

$$\eta_{ss}^{\Sigma}=0.048\,51(19)-0.1084(57)(R-2\text{ a.u.})+0.011\,816(R-2\text{ a.u.})^2,$$

$$\eta_{sd}^{\Sigma}=-0.013\,97(79)-0.001(15)(R-2\text{ a.u.})+0.011\,09(R-2\text{ a.u.})^2,$$

$$\eta_{dd}^{\Sigma}=0.1173(12)+0.1187(98)(R-2\text{ a.u.})+0.047\,661(R-2\text{ a.u.})^2,$$

$$\eta_{dd}^{\Pi}=0.073\,42(50)+0.0871(53)(R-2\text{ a.u.})+0.030\,152(R-2\text{ a.u.})^2,$$

$$\eta_{dd}^{\Delta}=-0.029\,07(53)-0.0537(90)(R-2\text{ a.u.})-0.003\,147(R-2\text{ a.u.})^2$$

(with numbers in parentheses representing standard errors in units of the last digit reported for the parameter.)

The *ab initio* MQDT results for the fitted rovibronic levels had a rms error of 1.8 cm^{-1}, which was reduced to 0.14 cm^{-1} by fitting the quantum defects. This was achieved by only marginal changes in the quantum-defect functions, with the largest change in equilibrium value being only 0.0018 for η_{sd}^{Σ}. The fitted quantum-defect functions are compared with the *ab initio* ones from RJ-I in Fig. 7. The fitted ones are only shown over a region of ± 0.3 a.u. around R_e, i.e., roughly the region of R explored by the $v=0$ vibrational levels included in the fitting.

Schins *et al.* [5] have used the coupled-equations approach to study the $n=3$ triplet gerade manifold. In their work the four vibrational matrix element functions, which arise from the electronic coupling between the s and d channels, are each modeled as a four-term series in Hermite polynomials and fitted to the experimental data of Alikacem and Larzillière [19]. These vibrational matrix elements are functions of R with very sharp peaks around the equilibrium geometry. Setting these functions to zero, and thus performing a pure *ab initio* calculation, "agreement with experiment down to 30 cm^{-1} was found" [5]. The current *ab initio* MQDT calculations for the triplet levels are therefore about an order of magnitude more accurate than the *ab initio* coupled-equations calculations of Schins *et al.* Bak and Linderberg [22] had earlier performed fully *ab initio* coupled-equations calculations of the $n=3$ triplet gerade manifold. Their results, however, were in disagreement with experiment by several hundreds of wave-number units.

By performing a least-squares adjustment of the 16 coefficients multiplying the Hermite polynomials used to describe the vibrational matrix element functions, Schins *et al.* obtained much better results. They tested the physicality of their fitted model by using the same parameters to calculate the equivalent energy levels of HD and D_2. The agreement with experiment for all three isotopes is of the order of one wave number, indicating the quality of their fitted model (see Appendix A for more discussion of

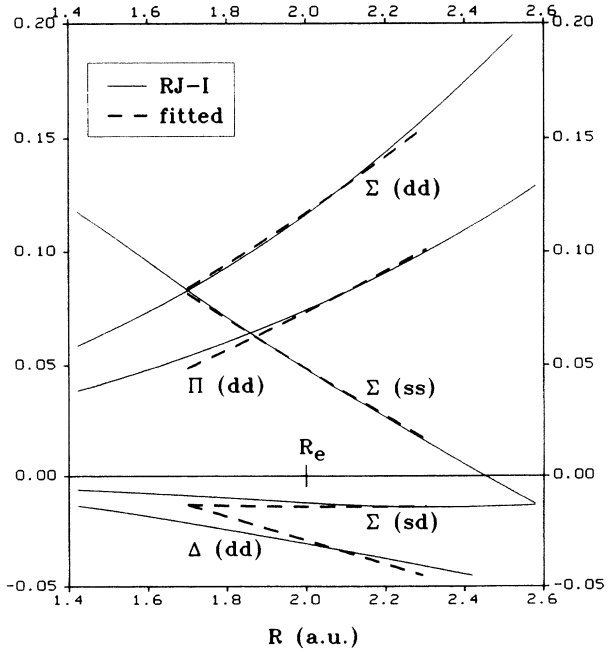

FIG. 7. Comparison of the fitted (dashed lines) triplet quantum-defect functions with the *ab initio* ones (solid curves).

this point).

Because of the different data sets used, it is not possible to make a direct comparison of the fitted MQDT results with those of the coupled-equations techniques. The rms error of the results obtained by Schins *et al.* for the $v=0$ levels they included in their fitting is 0.8 cm^{-1}. This is not as good as the 0.14-cm^{-1} rms error obtained with the MQDT approach. Their fitting, however, also included $v=1$, 2, and 3 states, and relied upon the data of Alikacem and Larzillière [19], which may be somewhat problematic, as discussed in the Appendix.

A striking feature of the *ab initio* MQDT and the coupled-equations calculations is that they both indicate that the $h2$ and $h3$ levels identified by Dieke [14] and Alikacem and Larzillière [19] are most likely incorrect. The various determinations of the $h2$ and $h3$ levels are compared in Table VII. It is clear that neither the present MQDT nor the fitted coupled-equations results are in agreement with the experimental energies. What is clear, however, is that the MQDT and coupled-equations results are in good agreement with each other. This despite the fact that the coupled-equations calculations are actually based on a fitting to the data of Ref. [19]. That the two very different theoretical models should agree with each other so well indicates that the experimental values for $h2$ and $h3$ are very likely incorrect, and that the true levels must lie relatively close to the theoretical ones.

Finally, it is worth pointing out that a distinct advantage of using the MQDT approach in a least-squares fitting is that the quantities being fitted are the quantum-defect functions which are smooth functions of R, rather than the very sharply peaked vibrational matrix element functions of the coupled-equations approach.

IV. CONCLUSION

In these three papers we have shown that MQDT provides a unified and quantitative description of all the gerade electronically excited singlet and triplet levels of H_2 up to within 0.2 eV of the $n=2$ dissociation limit. Except for the illustrative example in Sec. III C, these rovibronic calculations involved no adjustment of the parameters and thus represent a pure *ab initio* calculation of the gerade energy level spectrum of H_2 which completely avoids the detailed state-by-state evaluation of the rovibronic coupling. The success of the calculations not only confirms the quantum-defect theory approach used here, but also reconfirms the quality of the clamped-nuclei *ab initio* calculations from which the quantum defects were abstracted, in particular those of Wolniewicz and Dressler [3].

This work shows the feasibility of nonperturbative *rovibronic* MQDT, allowing for electronic excitation of the core. Owing to the $-1/R$ form of the EF potential-energy function in the region where it corresponds to the $H^+ + H^-$ ionic state, the vibrational level density increases in an analogous way to the increase in electronic state density in a Rydberg series. In the present calculation this manifests itself by the need for an extensive basis. This clearly points to the necessity for a channel treatment of the vibrational coordinate as well. This next phase of the work is in progress, and we anticipate that it will allow us to calculate all levels up to the $n=2$ dissociation limit and beyond, and thus to calculate resonances in the $H(1s)+H(n=2)$ vibrational continuum.

ACKNOWLEDGMENTS

S.C.R. thanks the Natural Sciences and Engineering Research Council of Canada, the ETH (Zürich), Professor Kurt Dressler, and the late Professor Fraser Birss for their support of this work. Professor Dressler is thanked for the provision of many results in advance of publication, and Professor Birss's useful comments with regard to aspects of rotational symmetry are fondly remembered. The hospitality of the Laboratoire Aimé Cotton du CNRS, Orsay, France, has been most helpful. Finally, Marta Wojnarowska is thanked for running some of the calculations.

TABLE VII. Comparison of experiment and theory for $h2$ and $h3$ levels.

	N	Observed[a]	MQDT[b]	CE[c]	Obs-MQDT[d]	Obs-CE[e]	CE-MQDT[f]
$h2$	0	116 284.06	116 326.95	116 331.11	−42.89	−47.05	4.16
	1	116 338.98	116 382.04	116 387.34	−43.06	−48.36	5.30
	2	116 448.39	116 491.68	116 498.97	−43.29	−50.58	7.19
	3	116 612.06	116 654.74	116 664.26	−42.68	−52.20	9.52
	4	116 827.15	116 869.50		−42.35		
	5	117 093.62	117 133.93		−40.13		
$h3$	0	118 271.10	118 363.13	118 359.57	−92.03	−88.47	−3.56
	1	118 323.81	118 414.82	118 411.34	−91.01	−87.52	−3.48
	2	118 428.79	118 517.75	118 514.37	−88.96	−85.58	−3.38
	3	118 585.19	118 671.04	118 667.64	−85.85	−82.45	−3.40

[a]Observed term energies (cm^{-1}) from Ref. [19].
[b]*Ab initio* calculated MQDT energies (cm^{-1}) from present work.
[c]Fitted coupled-equation energies (cm^{-1}) from Ref. [5].
[d]Observed minus MQDT (cm^{-1}).
[e]Observed minus coupled equations (cm^{-1}).
[f]Coupled equations minus MQDT (cm^{-1}).

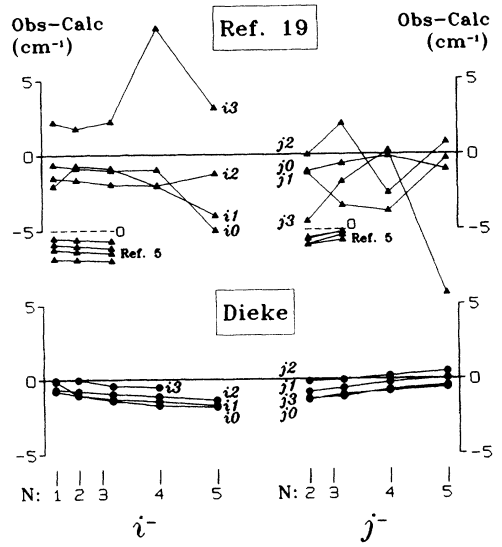

FIG. 8. Differences between experimental ("obs") and MQDT ("calc") term values for f levels of triplet i and j states. Reference [19] at top, and Dieke [14] at bottom. The difference between the fitted terms of Schins *et al.* [5] and the MQDT terms are also shown in the upper part, shifted down by 5 cm^{-1}, with dashed lines indicating the corresponding zero line.

APPENDIX

The manifold of triplet states has been recently reexamined by Alikacem and Larzillière [19]. However, it turns out that for the same levels the term values that they determined show greater scatter around our MQDT predicted values than do the much earlier term values of Dieke [14]. This is particularly evident in the f states to which $\Lambda=0$ does not contribute, so that electronic mixing is absent, as described in Sec. II. Thus only rotational channel interactions (l uncoupling) play a significant role. This simplicity leads to the MQDT calculations being especially accurate for these states. The differences between the observed and calculated term values are illustrated in Fig. 8. In this figure Dieke's term values are seen to be in excellent agreement with the current theoretical values, with the observed minus calculated differences exhibiting a very smooth variation with N. Alikacem and Larzillière's values, however, not only scatter more erratically, but also deviate from our MQDT predictions with a greater rms deviation: 3.0 cm^{-1} compared to the 1.0-cm^{-1} rms deviation of Dieke's data.

As discussed above, Schins *et al.* [5] fitted Alikacem and Larzillière's term values with a physically constrained model. The differences between their calculated term values and ours are also shown in Fig. 8 (shifted down by 5 cm^{-1} to avoid congestion). It is striking that these differences exhibit a much smoother variation with N than do the experimental data upon which their fitting was based. Indeed, their fitted term values are in better agreement with the current MQDT predictions (rms deviation 1.1 cm^{-1}) than are the experimental terms of Ref. [19] themselves (rms deviation of 1.9 cm^{-1} for the same levels). We have therefore not included data from Ref. [19] in our tables (except Table VII) and figures.

[1] S. C. Ross and Ch. Jungen, Phys. Rev. A **49**, 4353 (1994).
[2] S. C. Ross and Ch. Jungen, Phys. Rev. A **49**, 4364 (1994).
[3] K. Dressler (private communication).
[4] C. B. Wakefield and E. R. Davidson, J. Chem. Phys. **43**, 834 (1965).
[5] J. M. Schins, L. D. A. Siebbeles, J. Los, and W. J. van der Zande, Phys. Rev. A **44**, 4162 (1991).
[6] S. L. Guberman, J. Chem. Phys. **78**, 1404 (1983).
[7] K. Dressler and L. Wolniewicz, Can. J. Phys. **62**, 1706 (1984).
[8] W. Kołos and J. Rychlewski, J. Mol. Spectrosc. **66**, 428 (1977).
[9] W. Kołos and J. Rychlewski, J. Mol. Spectrosc. **91**, 128 (1982).
[10] J. Rychlewski, J. Mol. Spectrosc. **104**, 253 (1984).
[11] R. S. Mulliken, J. Am. Chem. Soc. **88**, 1849 (1966).
[12] G. Herzberg and Ch. Jungen, J. Chem. Phys. **84**, 1181 (1986).
[13] D. M. Bishop and L. M. Cheung, Mol. Phys. **65**, 679 (1988).
[14] H. M. Crosswhite, *The Hydrogen Molecule Wavelength Tables of Gerhard Heinrich Dieke* (Wiley, New York, 1972).
[15] R. S. Freund, T. A. Miller, R. Jost, and M. Lombardi, J. Chem. Phys. **68**, 1683 (1978).
[16] S. Yu and K. Dressler, J. Chem. Phys. (to be published).
[17] T. A. Miller and R. S. Freund, Adv. Magn. Res. **9**, 49 (1977).
[18] Ch. Jungen, I. Dabrowski, G. Herzberg, and M. Vervloet, J. Chem. Phys. **93**, 2289 (1990).
[19] A. Alikacem and M. Larzillière, J. Chem. Phys. **93**, 215 (1990).
[20] E. E. Eyler (unpublished).
[21] S. L. Bragg, J. W. Brault, and W. H. Smith, Ap. J. **263**, 999 (1982).
[22] K. L. Bak and J. Linderberg, J. Chem. Phys. **92**, 3668 (1990).

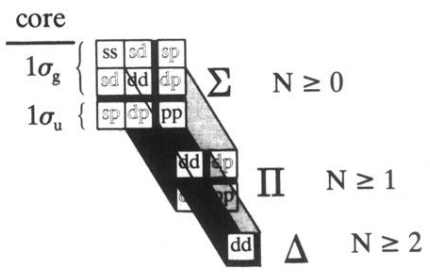

FIG. 1. Symbolized display of the electronic structure of the rovibronic K matrix [Eq. (4) of RJ-II]. See text for description.